

MERLOT:
A Model for Flow and Heat Transfer through
Porous Media for High Heat Flux Applications

A. R. Raffray and J. E. Pulsifer

November 2001



Fusion Division
Center for Energy Research

University of California, San Diego
La Jolla, CA 92093-0417

**MERLOT: A Model for Flow and Heat Transfer through Porous Media for
High Heat Flux Applications**

A. R. Raffray* and J. E. Pulsifer
Advanced Energy Technology Program
Center for Energy Research
University of California, San Diego
9500 Gilman Drive
EBU-II, Room 460
La Jolla, CA 92093-0417

Pre-print of paper submitted for publication in Fusion Engineering & Design

January 3, 2002

*phone: (858) 534-9720; fax: (858) 534-7716; e-mail: raffray@fusion.ucsd.edu

Abstract

Fusion power plant studies have found helium to be an attractive coolant based on its safety advantages and compatibility with structural materials at high temperature. However, gas coolants in general tend to provide modest heat transfer performance due to their inherently low heat capacity and heat transfer coefficient. Innovative techniques have been proposed previously using porous metal heat transfer media infiltrated by the coolant. The general design strategy is to minimize the coolant flow path length in contact with the porous medium, and to minimize the friction factor in that zone while simultaneously maximizing the heat transfer coefficient. In this work we seek to develop a comprehensive thermo-fluid model including all key heat transfer processes to help in assessing and optimizing a helium-cooled porous media configuration for plasma facing component application.

1. Introduction

Helium is an attractive coolant for fusion in-vessel components based on its safety advantages and compatibility with structural materials at high temperature. The maximum heat flux that can be accommodated is limited by the heat transfer coefficient achievable with flowing helium and the maximum allowable operating temperature of the structural materials. Helium flow through a simple channel provides limited heat transfer performance for fusion-relevant flow rates and pressure. This is acceptable for the first wall and blanket where the heat loads are moderate; however, in for the high heat load regions such as the divertor, accommodation of the high heat fluxes requires heat transfer enhancement features.

Porous metal heat exchangers have been studied in the past because of the large surface area they provide for heat transfer. For example, Thermacore has developed a porous metal heat exchanger applicable to fusion plasma-facing components [1,2]. A test article was fabricated and tested in the Sandia National Laboratory electron beam facility where it demonstrated relatively high overall heat transfer coefficients [2,3]. Such a configuration was also considered for the ARIES-ST divertor, as illustrated in Figure 1 [4]. The heat augmentation effect provided by this concept must be evaluated with respect to the associated pressure drop penalty. For a given particle dimension, the pressure drop through a porous medium is highly dependent on the porosity, ϵ , while the heat transfer coefficient tends to depend more on the specific surface area, S_p . In a conventional particle bed, S_p is directly related to ϵ through the following equation such that it becomes difficult to optimize the bed characteristics.

$$S_p = \frac{6(1 - \epsilon)}{d_p} \quad (1)$$

where d_p is the particle diameter.

Minimizing the flow path length as achieved in the concept shown in Fig. 1 does help to some extent to reduce the pressure drop penalty. As shown in Fig. 1, directing the flow through the porous medium around the circumference of the tube instead of along the length of the tube (~150 cm) as in the case of helium flowing in a simple channel, reduces the flow path length for the porous heat exchanger to ~80 mm.

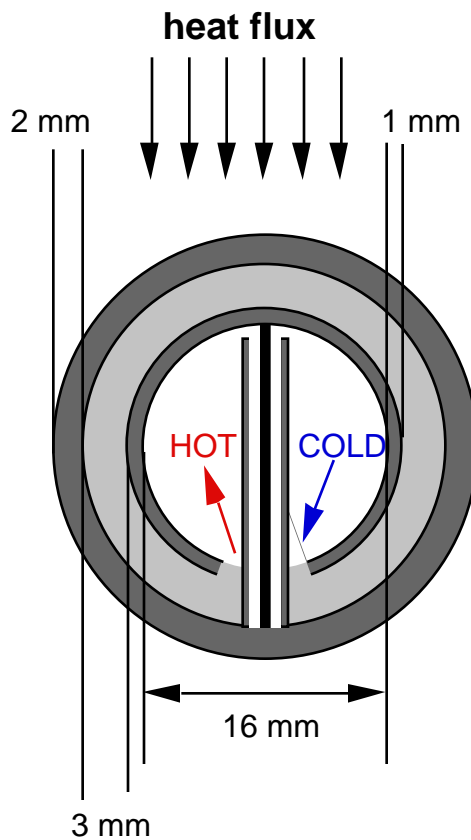


Figure 1 Schematic of a plasma divertor tube with 3-mm porous heat exchanger and inlet and outlet helium headers separated with thermal insulation, proposed for ARIES-ST. The design heat flux normal to the tube is 5 MW/m² [4].

An innovative design solution is based on a porous material using non-spherical fibers where the porosity and specific surface area can be optimized beyond their conventional particle bed dependence. Such a porous foam would have high porosity (which governs the pressure drop) but with specific surface area (influencing the heat transfer) higher than those that a conventional packed bed can provide. This could open up the window of application of helium for high heat flux fusion applications. Similar foams have already been manufactured. For example, Ultramet has proposed a new class of open cell, low density, high-temperature performance refractory foams for a variety of aerospace and industrial applications, as illustrated in Figure 2 [5]. These foams can be fabricated from any material or material combination (either homogeneously combined or layered) which can be deposited by CVD/CVI. Among the materials that can be deposited are the refractory metals, including tungsten, which is of particular interest for fusion applications. These cellular materials can be optimized for various properties (including porosity characteristics) simultaneously, can be furnished in various sizes and configurations, and are easy to machine. Face sheets of either the same or different material can be applied. Such a tungsten foam could be used either with two tungsten facesheets in a divertor design using tungsten as structural material (requiring high temperature operation, $> \sim 800^{\circ}\text{C}$, to avoid tungsten embrittlement) or, in a more conventional design, could be joined to a tungsten face sheet at the high temperature region and to the structural ferritic steel at the lower temperature region. This would open the door for higher allowable heat flux for the helium-cooled concept while maintaining the safety advantages of using an inert gas as coolant.

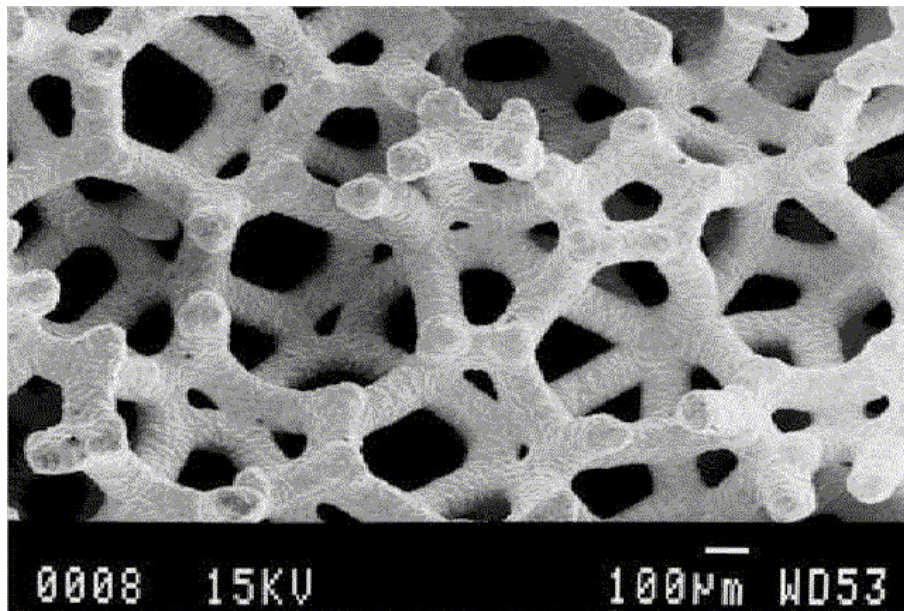


Figure 2 Example of Ultramet refractory foam [5].

This work focused on developing an improved phenomenological thermo-fluid model in order to assess and optimize such porous heat transfer media with the intent of guiding the direction of future modeling, material and experimental R&D.

2. Model Development

Most existing models for heat transfer through a porous medium seem to be based on a semi-empirical approach such as the following circuit-based model described in [2].

$$h_{eff} = \left(\varepsilon h_p + \frac{1}{R_o + \frac{1}{\sqrt{h_p k_p S_p} \tanh \sqrt{\frac{h_p S_p}{k_p} t}}} \right) \quad (2)$$

where h_p is the local particle-to-fluid heat transfer coefficient, R_o is the porous medium/wall interface resistance, k_p is the porous medium thermal conductivity and t is the porous medium thickness.

Such a model provides a quick and convenient means for estimating the overall heat transfer coefficient but is limited in its range of application, in particular to account for cases with large spatial variation of the microstructure characteristics (e.g. the porosity and directional thermal conductivity), for cases with high porosity, and/or for design configurations where entrance effects plays a major role. It would be very useful to develop a more comprehensive and fundamental model which first calculates the velocity profile and then the corresponding temperature distribution in the porous region, with the capability to account for microstructure variation and to include potentially important processes such as the local heat transfer between solid and fluid and the effect of dispersion. Such a model would provide a much better tool to perform a more detailed assessment and optimization of porous media for high heat flux application. This was the aim of this work and the proposed model is called MERLOT :

Model of
Energy-transfer
Rate for
flow in

Open-porosity
Tailored-media

First, the continuity equation and the modified Darcy equation including Forcheimer’s drag term and Brinkman’s viscosity term are used in estimating the velocity profile [6]. The thermal performance of porous media in an entrance region can be substantially dependent on the thermal development length. The temperature calculation must then be done in multi-dimensions. However, the velocity profile development plays a lesser role and tends to be very short when compared to flow through a regular channel. Consequently, for simplicity, fully-developed steady state flow was assumed for the solution of the continuity modified Darcy equations, which through a cylindrical geometry such as shown in Figure 3, can be expressed as:

$$\frac{\partial V_{\theta}}{\partial \theta} = 0 \tag{3}$$

$$0 = -\frac{1}{r} \frac{\partial P}{\partial \theta} - \frac{\mu}{K} V_{\theta} - \frac{\rho_f C}{\sqrt{K}} V_{\theta}^2 + \mu_{eff} \frac{\partial}{\partial r} \frac{1}{r} \frac{\partial}{\partial r} (r V_{\theta}) \tag{4}$$

where V_{θ} is the superficial velocity in the θ direction, P the fluid pressure μ the fluid viscosity; K the porous medium permeability, ρ_f the fluid density, and C the inertia coefficient.

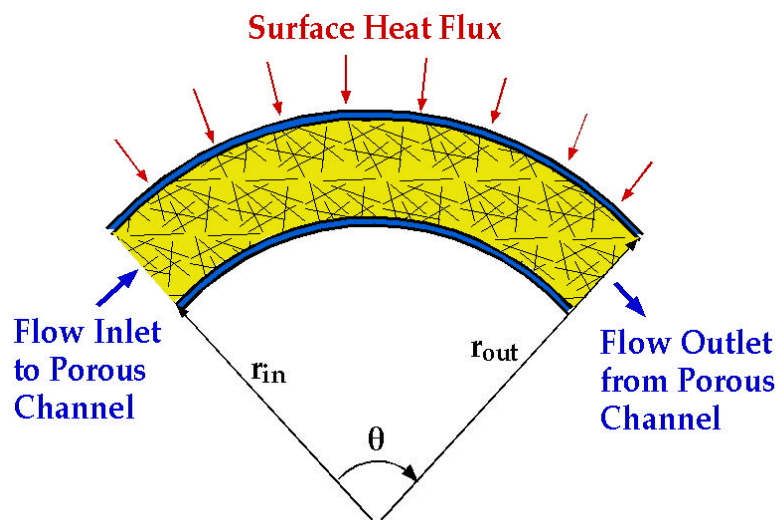


Figure 3 Model geometry for flow through porous media

Eq. (4) can be non-dimensionalized as follows, where the primes refer to non-dimensionalized variables and $v_{\theta 0}$ and P_o are the reference Darcy velocity and pressure, respectively.

$$r' = \frac{r}{r_{out}} \quad (5)$$

$$V'_{\theta} = \frac{V_{\theta}}{V_{\theta 0}} \quad (6)$$

$$P = \frac{P - P_0}{\rho_f V_{\theta 0}^2} \quad (7)$$

$$0 = -\frac{1}{r'} \frac{\partial P'}{\partial \theta} - \frac{V'_{\theta}}{\text{Re}_{ch} Da} - \frac{CV_{\theta}^2}{\sqrt{Da}} + \frac{1}{\text{Re}_{ch}} \frac{\partial}{\partial r'} \left(\frac{1}{r'} \frac{\partial}{\partial r'} (r' V'_{\theta}) \right) \quad (8)$$

where the Darcy number, Da , and Reynolds number for the channel, Re_{ch} are defined as:

$$Da = \frac{K}{r_{out}^2} \quad (9)$$

$$\text{Re}_{ch} = \frac{\rho_f V_{\theta 0} r_{out}}{\mu_{eff}} \quad (10)$$

An implicit finite difference scheme is used to solve Eq. (8) in combination with a tri-diagonal matrix solver subroutine using the Thomas algorithm [7]. The non-dimensional pressure gradient is assumed constant and set as input and the boundary conditions are no slip at both walls (i.e. $V'_{\theta, wall} = 0$). Due to the non-linear velocity term in Eq. (8), an iterative procedure is used to advance the solution by using the old value of velocity to compute the new ones until the desired convergence is reached.

Next, the 2-D temperature distribution can be obtained by separately solving the energy equations for the solid phase and the fluid phase, using a local heat transfer coefficient, h_c , at the interface between solid and fluid [6]. The equations are expressed so as to include the effect of spatial variations of thermal conductivity and porosity.

$$0 = \frac{1}{r} \frac{\partial}{\partial r} \left(r(1-\varepsilon)k_{s,r} \frac{\partial T_s}{\partial r} \right) + \frac{1}{r^2} \frac{\partial}{\partial \theta} \left((1-\varepsilon)k_{s\theta} \frac{\partial T_s}{\partial \theta} \right) + (1-\varepsilon)q'''_s + h_c S_p (T_f - T_s) \quad (11)$$

$$\rho_f C_{p_f} \frac{V_\theta}{r} \frac{\partial T_f}{\partial \theta} = \frac{1}{r} \frac{\partial}{\partial r} r \varepsilon k_{f,t,r} \frac{\partial T_f}{\partial r} + \frac{1}{r^2} \frac{\partial}{\partial \theta} \varepsilon k_{f,t,\theta} \frac{\partial T_f}{\partial \theta} + \varepsilon q'''_f + h_c S_p (T_s - T_f) \quad (12)$$

where ε is the porosity; $k_{s,r}$ and $k_{s,\theta}$ the solid thermal conductivities in the r and θ direction, respectively; T_s and T_f the solid and fluid temperatures, respectively; q'''_s and q'''_f the volumetric heat generations in the solid and fluid, respectively; S_p the specific surface area of the porous medium; ρ_f the fluid density; C_{p_f} the fluid heat capacity; and $k_{f,t,r}$ and $k_{f,t,\theta}$ the total effective fluid thermal conductivities in the r and θ direction, respectively.

h_c has been correlated from experimental data as a function of the Reynolds number, Re_{dp} , based on the pebble diameter and of the Prandtl number for pebble beds and can be expressed as [8]:

$$h_c = \frac{0.0036 Re_{dp}^{1.4} Pr^{0.333} k_{f,r}}{d_p} \quad (13)$$

$k_{f,t,r}$ and $k_{f,t,\theta}$ include the fluid thermal conductivity itself (k_f) and the enhancement provided by dispersion effects ($k_{disp,r}$ and $k_{disp,\theta}$) [9].

$$k_{f,t,r} = k_f + k_{disp,r}; k_{f,t,\theta} = k_f + k_{disp,\theta} \quad (14)$$

The dispersion effect tends to be more pronounced in the direction perpendicular to the flow than in the axial direction and, for a pebble bed can be expressed as a function of the local porosity, ε_i , Prandtl number and Reynolds number, $Re_{d,i}$ (based on the local velocity and porous medium characteristic dimension) and Peclet number [9]:

$$k_{disp} = 0.04 \frac{(1 - \varepsilon_i)}{\varepsilon_i} Re_{d,i} Pr k_{f,r} \quad (15)$$

Eqs. (11) and (12) can be non-dimensionalized as follows, where again the primes refer to non-dimensionalized variables and T_h and T_c refer to the cold and hot reference temperatures, respectively. The property data and the heat generation values are all non-dimensionalized by using reference values (denoted with the subscript *ref*).

$$T'_s = \frac{T_s - T_c}{T_h - T_c}; T'_f = \frac{T_f - T_c}{T_h - T_c} \quad (16)$$

$$k'_s = \frac{k_s}{k_{s,ref}}; k'_f = \frac{k_f}{k_{f,ref}} \quad (17)$$

$$\rho'_f = \frac{\rho_f}{\rho_{f,ref}} \quad (18)$$

$$Cp'_f = \frac{Cp_f}{Cp_{f,ref}} \quad (19)$$

$$q'_s = \frac{q'''_s}{q'''_{ref}}; q'_f = \frac{q'''_f}{q'''_{ref}} \quad (20)$$

$$h'_c = \frac{h_c S_{BET} (T_h - T_c)}{q'''_{ref}} \quad (21)$$

The following parameters, J_s , $J_{f,1}$ and $J_{f,2}$ are introduced to simplify the equation display:

$$J_s = \frac{k_{s,ref} (T_h - T_c)}{r_{out}^2} \quad (22)$$

$$J_{f,1} = \frac{k_{f,ref} (T_h - T_c)}{r_{out}^2} \quad (23)$$

$$J_{f,2} = \frac{\rho_{f,ref} Cp_{f,ref} V_{\theta_0} (T_h - T_c)}{r_{out}} \quad (24)$$

$$0 = J_s \frac{1}{r'} \frac{\partial}{\partial r'} r' k'_{s,r} (1-\varepsilon) \frac{\partial T'_s}{\partial r'} + \frac{1}{r'^2} \frac{\partial}{\partial \theta} k'_{s,\theta} (1-\varepsilon) \frac{\partial T'_s}{\partial \theta} + (1-\varepsilon) q'''_{ref} q'''_s + q'''_{ref} h'_c (T'_f - T'_s) \quad (25)$$

$$J_{f,2} \rho'_f Cp'_f \frac{V'_\theta}{r'} \frac{\partial T'_f}{\partial \theta} = J_f \frac{1}{r'} \frac{\partial}{\partial r'} r' k'_{f,t,r} \varepsilon \frac{\partial T'_f}{\partial r'} + \frac{1}{r'^2} \frac{\partial}{\partial \theta} k'_{f,t,\theta} \varepsilon \frac{\partial T'_f}{\partial \theta} + \varepsilon q'''_{ref} q'''_f + q'''_{ref} h'_c (T'_s - T'_f) \quad (26)$$

The above equations are expressed in general terms to include the effect of porosity variation in both r and θ directions.

Eqs. (25) and (26) are solved based on an implicit alternating direction finite difference scheme using the velocity distribution from the solution of Eq. (8) as input and based on the following boundary conditions[7]:

- At inlet, $\theta = 0$, the temperature is set at the uniform inlet temperature; and
- At outlet, $\theta = \theta_{out}$ for simplicity, adiabatic conditions are assumed.
- At both walls, $r=r_{in}$ and $r=r_{out}$, the boundary conditions are set by equating the total heat flux, q''_w to the combined fluid and solid heat fluxes. For example, for the inner wall the boundary condition is:

$$q''_w = -(1-\varepsilon)k_{s,r} \frac{\partial T_s}{\partial r} - \varepsilon k_{f,t,1} \frac{\partial T_f}{\partial r} \quad \text{innerwall} \quad (27)$$

$k_{f,t,1}$ in the equation represents an effective conductivity for the fluid at the wall including a convection component averaged over the radial increment at the wall.

Eq. (27) can be written in non-dimensional form as follows:

$$q'_w q''_{w,ref} = -\frac{(T_h - T_c)}{r_{out}} (1-\varepsilon)k_{s,ref} k'_{s,r} \frac{\partial T'_s}{\partial r'} - \varepsilon k_{f,ref} k'_{f,t,1} \frac{\partial T'_f}{\partial r'} \quad \text{innerwall} \quad (28)$$

where the wall heat flux is non-dimensionalized based on a reference value:

$$q'_w = \frac{q''_w}{q''_{w,ref}} \quad (29)$$

The solution proceeds iteratively. First, tri-diagonal matrix equations for the temperature in the r direction along each successive theta plane are solved using the old temperature values in the theta direction terms. Next, similar tri-diagonal matrix equations but for the temperature along the theta direction are solved using the just computed temperature values in the r -direction. The program iterates in these alternating direction solutions until the desired convergence is achieved.

3. Model Validation

The model was seen to provide consistent and qualitatively correct results for both the velocity profiles and temperature profiles based on expected results for given porosity variations. It was difficult to find from the literature results for curved geometry for final confirmation of the results. An example set of results that were found were from Cheng and Hsu who considered the variation in porosity for a packed-sphere bed and calculated the wall channeling effect on axial velocity for an annular geometry with flow in the axial direction and assuming only the Brinkman viscous effect but not the Forcheimer inertial effects [10]. They used the following expressions to estimate the porosity variation in the direction perpendicular to the flow:

$$\varepsilon = \varepsilon_{\text{inf}} \left[1 + C_1 \exp \left(-N_1 \frac{(r_{\text{out}} - r)}{d_p} \right) \right] \quad \text{for } 0.5(r_{\text{out}} - r_{\text{in}}) \leq r \leq r_{\text{out}} \quad (30)$$

$$\varepsilon = \varepsilon_{\text{inf}} \left[1 + C_1 \exp \left(-N_1 \frac{(r - r_{\text{in}})}{d_p} \right) \right] \quad \text{for } r_{\text{in}} \leq r \leq 0.5(r_{\text{out}} - r_{\text{in}}) \quad (31)$$

where $C_1=1$ and $N_1=2$ for a bulk porosity, ε_{inf} of 0.4 [10].

For a particle bed, consistent with the Ergun and Kozeny equations, the permeability is given by [6,8]:

$$K = \frac{d_p^2 \varepsilon^3}{A(1 - \varepsilon)^2} \quad (32)$$

where A is a shape factor (=150).

MERLOT was run with a large aspect ratio over a short angle to simulate flow in a straight channel for conditions similar to those used in Ref. [10] including the above porosity and permeability equations, and setting the inertia coefficient, $C=0$ in eq. (4) to exclude the Forcheimer effect. The resulting velocity profiles compared reasonably well with Cheng and Hsu's results given the inherent differences in geometry, as illustrated in Fig. 4 for a case with a $\frac{d_p}{r_{\text{in}}}$ of 0.085.

The energy part of the code was validated by comparing the temperature distribution for simple cases involving heat fluxes at the wall or heat generation in the solid to predicted profiles. Also,

conservation of energy was verified for a number of set cases to ascertain the code robustness in analyzing cases with different geometries, heat inputs, and porous microstructure. This was assessed by comparing the energy transferred to the coolant between inlet and outlet to the energy input either through the wall heat flux or volumetric heat generations. In all cases an energy balance was achieved to a reasonable level (within a few %) by refining the mesh and convergence criterion.

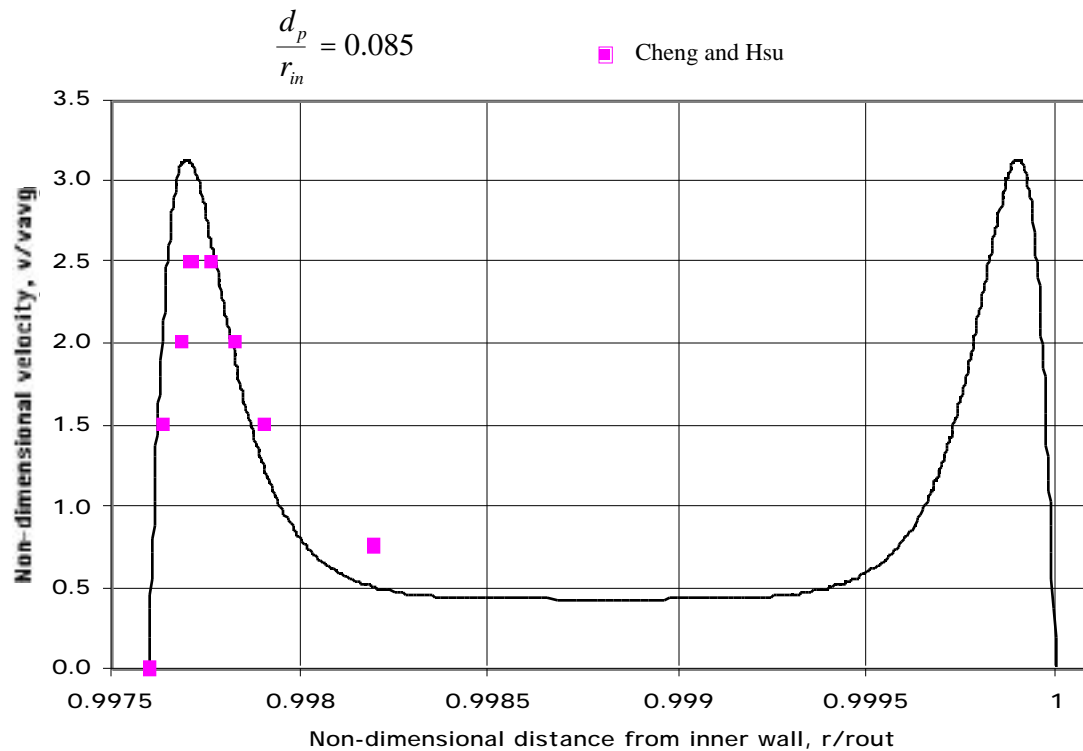


Figure 4 Comparison of velocity profile computed from MERLOT to the results from Cheng and Hsu [10].

Experimental results on the thermal performance of porous media under high heat flux are scarce and existing data, such as reported in Ref. [3] tend to provide global measurement of the effective heat coefficient based on the heat flux and the inlet and outlet temperature but lack detailed measurements of the temperature distribution in the wall and of the thermal and velocity profiles in the porous media. Thus, it is difficult to further validate the model based on existing experimental data for divertor-like conditions. Instead, parametric studies were conducted to guide the optimization of the porous medium configuration and to help in defining future high heat flux dedicated experiments.

4. Porous Media Analysis

4.1 Calculation Procedure and Example 3-D Temperature Distribution

The MERLOT calculations proceeded as follows:

1. The He mass flow rate corresponding to a given He temperature rise and a given heat input is calculated.
2. The pressure gradient, $\frac{dP}{dx}$, corresponding to the calculated He mass flow rate, average porosity, and particle diameter is estimated from the well-known Ergun equation for a packed bed [1,6].

$$\frac{dP}{dx} = 150 \frac{(1-\epsilon)^2}{\epsilon^3} \frac{\mu V_0}{(\varphi d_p)^2} + 1.75 \frac{(1-\epsilon)}{\epsilon^3} \frac{\rho_f V_0^2}{\varphi d_p} \quad (33)$$

where μ_f is the fluid viscosity; V_0 the superficial velocity, φ = particle shape factor, and ρ_f the fluid density. This expression implies an inertia coefficient, C , given by:

$$C = \frac{1.75(1-\epsilon)}{\epsilon^3 d_p} \quad (34)$$

3. The correct velocity profile corresponding to this pressure gradient and to the porosity spatial distribution is then computed.
4. Finally, the corresponding 2-D temperature distribution in the solid and fluid is calculated, yielding the exact He outlet temperature.

Figure 5 shows an example temperature distribution output from MERLOT that corresponds to the ARIES-ST divertor and the dimensions shown in Fig. 1 [4]. The model considered the top half (=0 to =) of the tube of outer and inner radii 12 and 9 mm, respectively subjected to a 5 MW/m² heat flux. The He inlet pressure is 4 MPa and its inlet and outlet temperatures are 350°C and 650°C, respectively. Tungsten is considered as solid material and its thermal conductivity was set at 100 W/m-K and the porous medium characteristic dimension is 0.2 mm. The bulk porosity is 40% and the porosity variation is based on Eqs. (30) and (31). For simplicity in this example case,

no thermal dispersion effect was assumed and convection between solid and fluid at the wall and in the bulk was assumed very high. The temperature gradient in the radial direction is governed by heat diffusion from the heat flux at the outer wall, the total heat input dictating the temperature rise along the flow direction () showing the set input inlet and outlet temperatures of 350°C and 650°C, respectively.

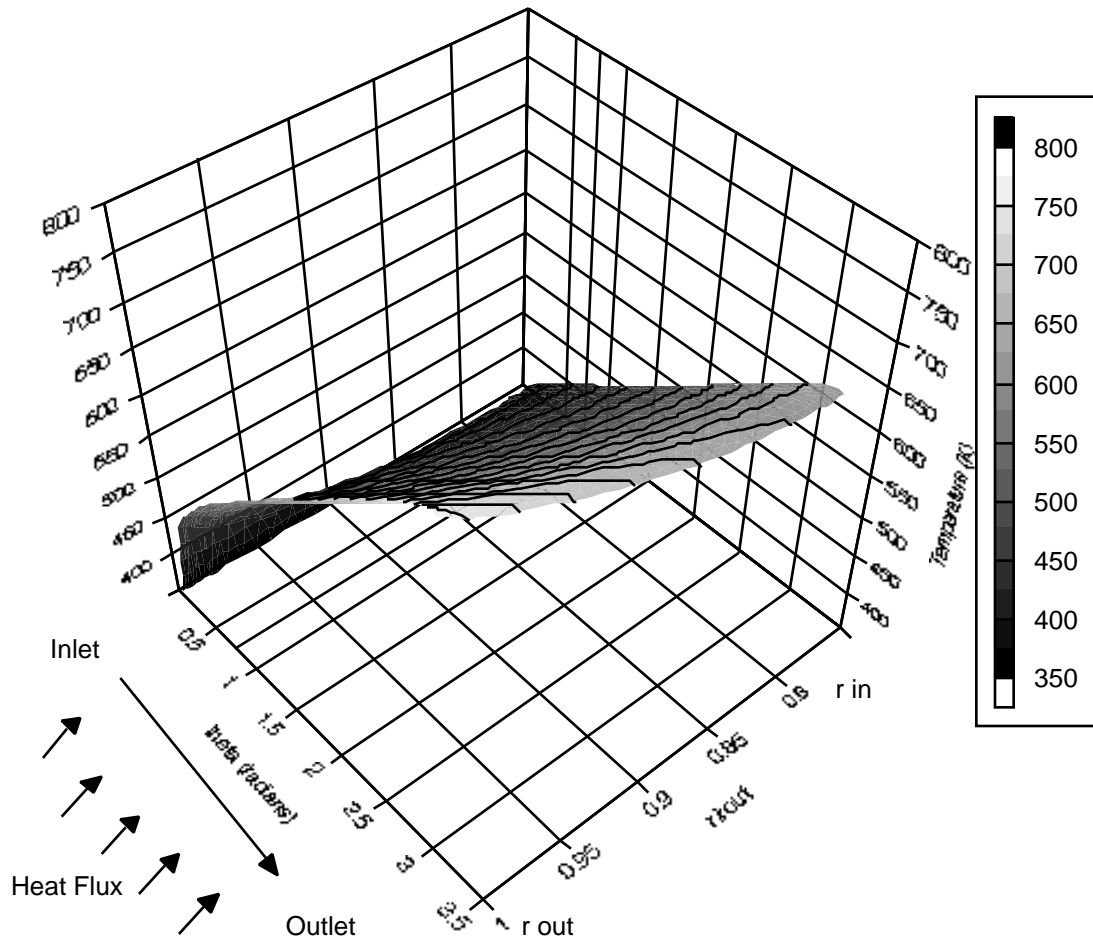


Figure 5 Temperature distribution in porous bed channel for a bulk porosity of 0.4 and a solid thermal conductivity of 100 W/m-K.

4.2 Parametric Studies

While MERLOT can model situations that include porosity variation, such as that found at the wall of a packed bed, it does not include terms for contact resistance between particles. Therefore, MERLOT is more suitable for analyzing materials such as metal foams and engineered fibers whose models do not rely strongly on particle-to-particle contact. In the following parametric studies, MERLOT is used with isotropic porosity. Isotropic porosity is not a requirement for metal foams or ordered fibers, but is a simplification that could later be lifted in order to experiment with

deliberate porosity variation, or material tailoring. In the absence of specific data for the cases analyzed, the specific surface area is estimated based on the bulk porosity and porous medium characteristic dimension based on Eq (1). The Carman-Kozeny model for permeability (see Eq. (32)) is assumed although its applicability for high porosities should be further verified, and Ergun's equation is used to estimate the initial pressure drop. Eq.(13) was used to estimate the local heat transfer coefficient at the wall and between solid and fluid in the porous region. It is not clear how accurate the dispersion model (Eq. 15) is for higher porosity cases and, for simplicity and to avoid leaving too many potentially uncertain variable parameters, thermal dispersion was not included in these initial parametric studies. However, the effects on the results of including dispersion and also of varying the heat transfer coefficient between solid and flowing fluid were parametrically evaluated and are discussed in Section 4.2.3.

Modifications to these models can be easily implemented if different expressions for the above-defined parameters are deemed more appropriate. For these parametric studies performed to help define the characteristics of attractive porous media for high heat flux application, trends are more important than achieving high accuracy of absolute values and these assumptions are judged reasonable.

Table 1. Parameters used for parametric studies.

Fluid	He
Fluid properties	Varied as $f(T)$
He inlet pressure, P_{in}	4 MPa
He inlet temperature, T_{in}	823 K
He outlet temperature, T_{out}	various
Solid thermal conductivity, k_s	50-200 W/m-K
Porous medium characteristic dimension, d_{char}	0.1 mm (unless noted)
Bulk porosity,	various
Porosity variation in bulk	constant
Inner radius, r_{in}	9 mm (unless noted)
Outer radius, r_{out}	12 mm (unless noted)
Heat flux, q''	5 and 30 MW/m ²

Table 1 summarizes the parameters used for the parametric studies. They are similar to those used for the ARIES-ST example case. The top half of the tube ($\theta = 0$ to $\theta = \pi$) is subjected to a heat flux; two bounding values were assumed: 5 and 30 MW/m² representing lower and upper reference values for divertor application. The solid thermal conductivity, k_s , is assumed constant for each run.

As a measure of the heat transfer performance, an effective heat transfer coefficient, h_{eff} is calculated at each location along the heated wall by dividing the applied heat flux by the difference between the wall temperature and the average coolant temperature at this location. Figure 6 shows an example of a typical variation of h_{eff} with θ for a case with a 30 MW/m² applied heat flux and a uniform porosity of 0.8, for different He bulk temperature rises (which for the given heat flux dictates the average velocity). h_{eff} is much higher at the entrance and decreases to a constant value as the flow becomes thermally developed. This indicates the attractiveness of designing for high heat flux accommodation close to the entrance region. However, when evaluating different configurations, the effective heat transfer coefficient at the coolant outlet should be chosen as a reasonable comparative measure of heat transfer performance.

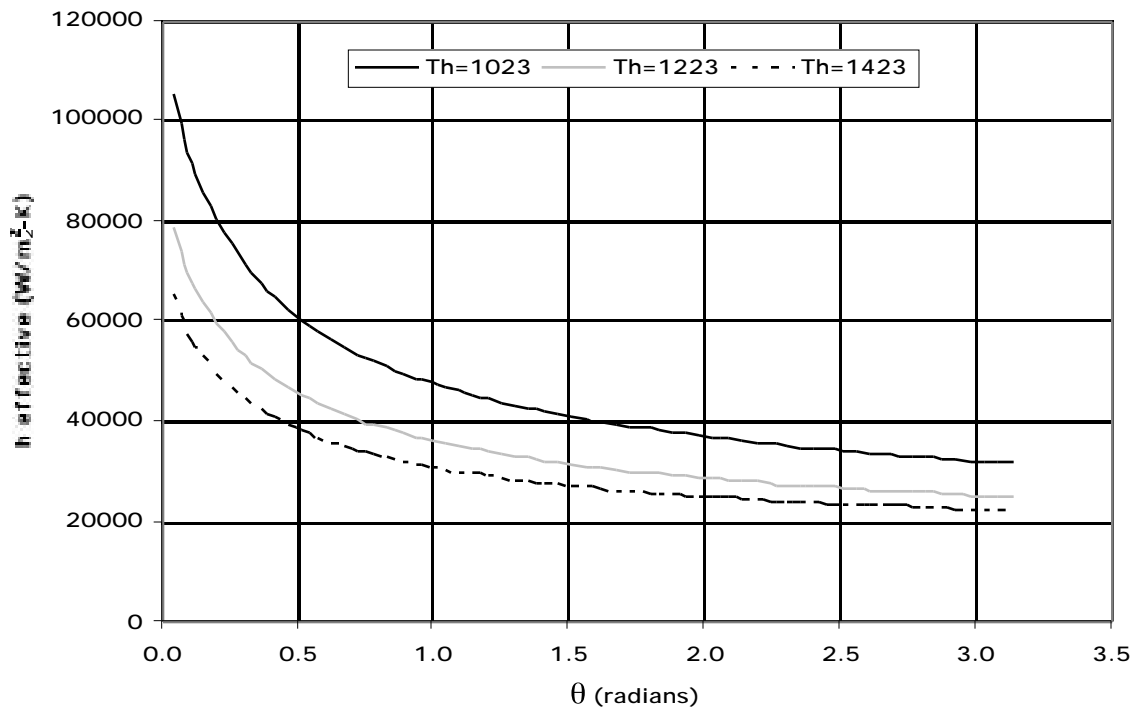


Figure 6 Variation of local effective heat transfer coefficient with radial angle along the flow path for different He bulk temperature rises ($q''=30$ MW/m², $\phi=0.8$, $d_{char}=0.1$ mm, $k_s=100$ W/m-K, $T_{in}=823$ K).

4.2.1 Porosity and Velocity

The parametric studies started by investigating the effect on heat transfer performance of changing the bulk porosity. Figure 7 shows the variation of the effective heat transfer coefficient with porosity as calculated by MERLOT for a heat flux of 5 MW/m^2 and for different solid thermal conductivities. h_{eff} decreases with increasing porosity approaching the regular channel value at 100% porosity. The solid thermal conductivity has an important effect on the effective heat transfer coefficient in particular at lower porosities. If allowed by the choice of solid material, increasing the solid thermal conductivity is highly desirable since it does not adversely affect the pressure drop while increasing the effective heat transfer coefficient.

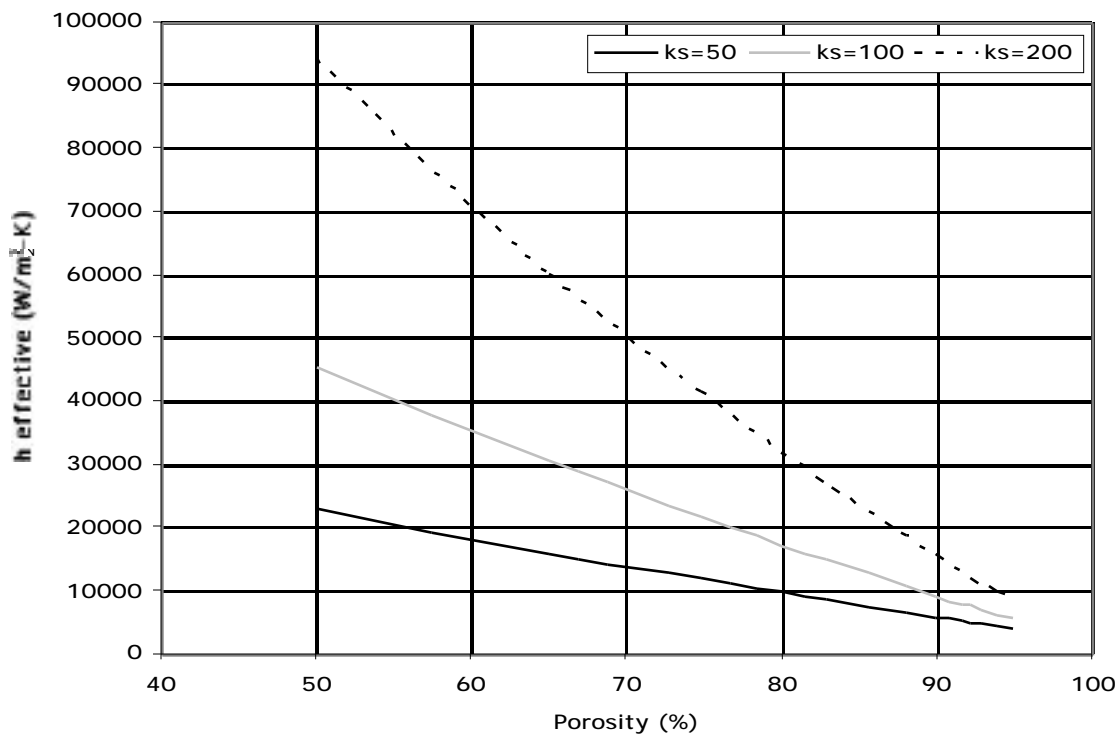


Figure 7 Effective heat transfer coefficient ($\text{W/m}^2\text{-K}$) at outlet as a function of porosity for different solid thermal conductivities ($q''=5 \text{ MW/m}^2$, $d_{\text{char}}=0.1 \text{ mm}$, He $T_{\text{in}}=823\text{K}$, He $T_{\text{out}}=1223\text{K}$).

Figure 8 shows the variation of h_{eff} with velocity (or He temperature rise for a given heat flux) for different porosity values for $q''=5 \text{ MW/m}^2$. h_{eff} increases with velocity but decreasingly so at higher velocities where the fluid contribution to the overall heat transfer is high enough that conduction through the solid becomes the limiting factor. Figure 9 shows the corresponding maximum wall temperature at the interface with the fluid outlet which when added to the

temperature rise through the armor yields an estimate of the corresponding maximum armor temperature. As an example, for a 3-mm tungsten armor with $k_s = 100 \text{ W/m-K}$ under a heat flux of 5 MW/m^2 , the temperature rise through the tungsten is 143K which can be added to the temperature values shown in Fig. 9 to estimate the maximum tungsten armor temperature.

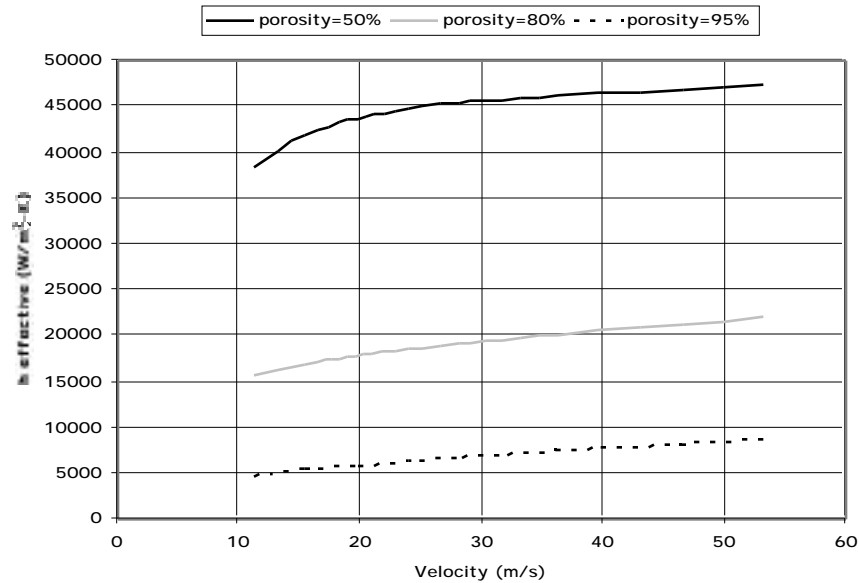


Figure 8 Effective heat transfer coefficient ($\text{W/m}^2\text{-K}$) at outlet as a function of velocity for different porosities ($q''=5 \text{ MW/m}^2$, $d_{\text{char}}=0.1 \text{ mm}$, $k_s=100 \text{ W/m-K}$, He $T_{\text{in}}=823\text{K}$).

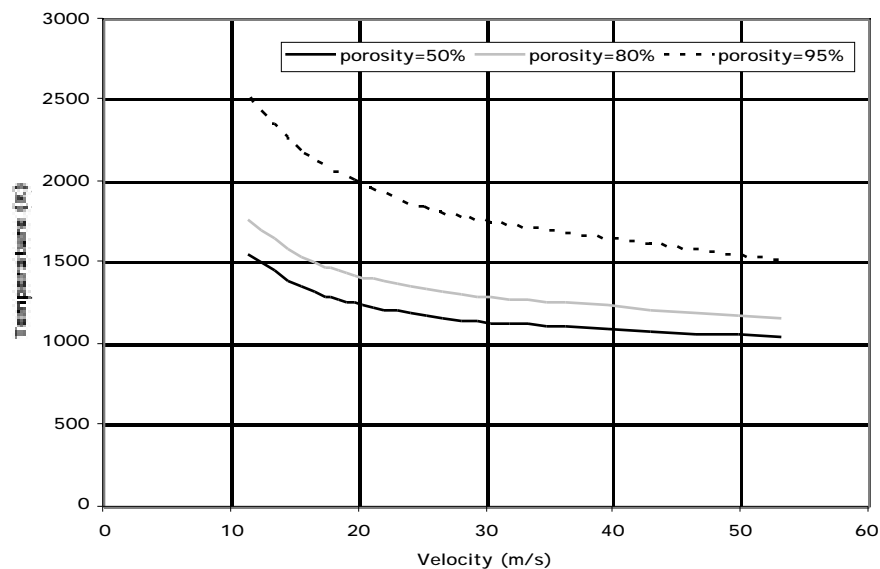


Figure 9 Maximum wall temperature (K) at the fluid outlet interface as a function of velocity for different porosities ($q''=5 \text{ MW/m}^2$, $d_{\text{char}}=0.1 \text{ mm}$, $k_s=100 \text{ W/m-K}$, He $T_{\text{in}}=823\text{K}$).

Figure 10 shows the variation of the He pressure drop, P , with velocity corresponding to the previous case. P increases exponentially with velocity and is much higher for cases with lower porosities.

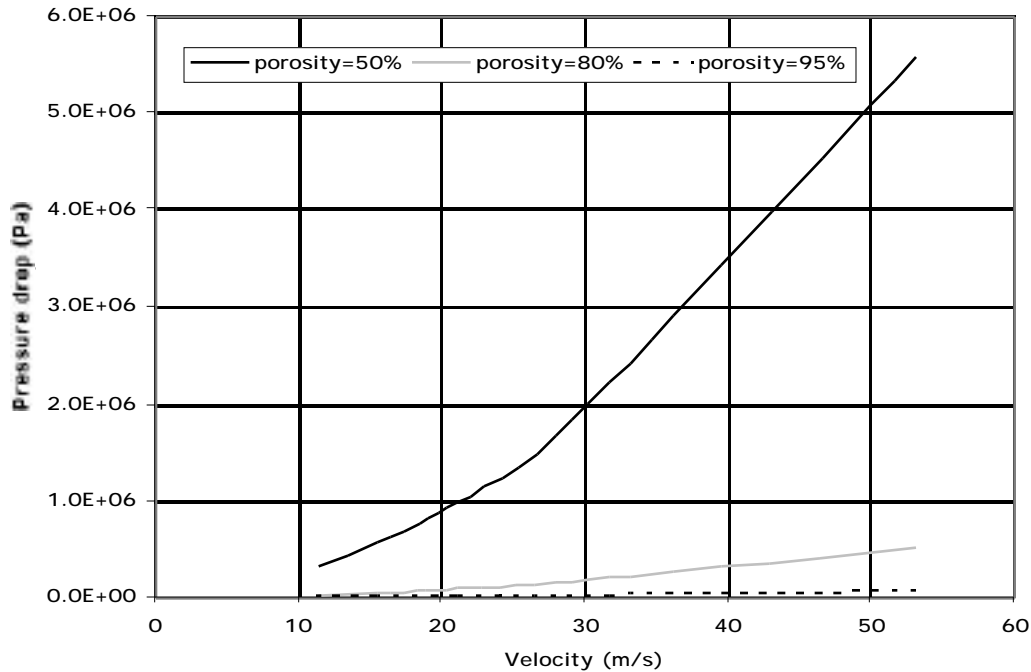


Figure 10 Pressure drop (Pa) as a function of velocity for different porosities ($q''=5 \text{ MW/m}^2$, $d_{\text{char}}=0.1 \text{ mm}$, He $T_{\text{in}}=823\text{K}$).

The design optimization must then balance the heat transfer performance for the given porous configuration with the pressure drop penalty. An interesting performance to penalty measure is the ratio of effective heat transfer coefficient to pressure drop, which is shown as a function of velocity in Figure 11. This ratio is much higher at lower velocities and decreases rapidly with velocity, indicating the benefit of optimization at the lowest possible velocity. Interestingly, it also indicates the benefit of optimization at the highest possible porosity as the ratio decreases sharply with decreasing porosity.

Similar cases were run for a heat flux of 30 MW/m^2 . Figure 12 shows the variation of h_{eff} with velocity (or He temperature rise for a given heat flux) for different porosity values for $q''=30 \text{ MW/m}^2$. Figure 13 shows the corresponding variation of pressure drop with velocity and Figure 14 shows the variation of the ratio of h_{eff} to P with velocity for different porosities. For the 30 MW/m^2 case the velocities are much higher than for the 5 MW/m^2 case for given coolant

temperature rises. Thus, the corresponding h_{eff} and pressure drop values are higher but the variations are similar to the previous cases and the same types of observation can be made.

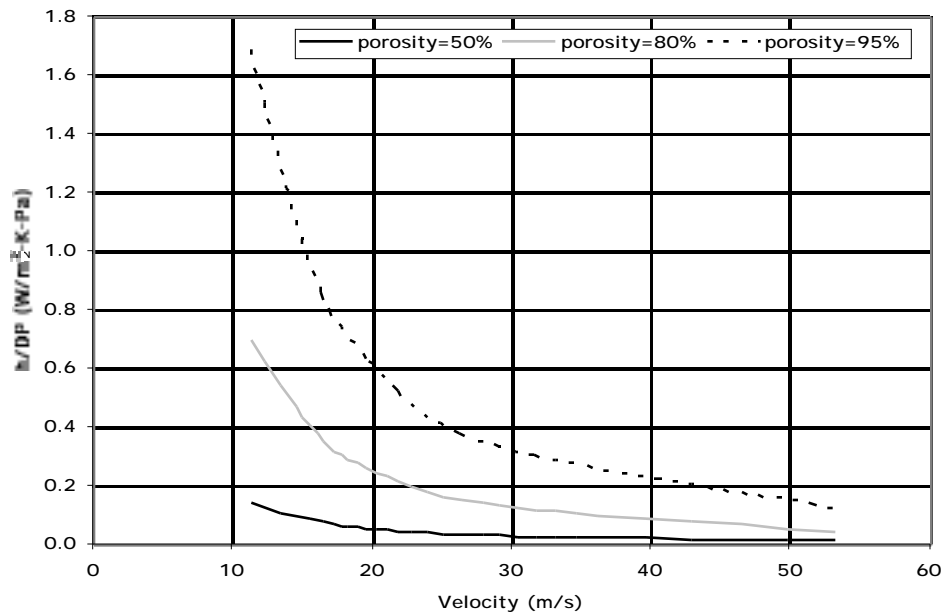


Figure 11 Ratio of effective heat transfer coefficient at outlet to pressure drop as a function of velocity for different porosities ($q''=5 \text{ MW/m}^2$, $d_{\text{char}}=0.1 \text{ mm}$, $k_s=100 \text{ W/m-K}$, He $T_{\text{in}}=823\text{K}$).

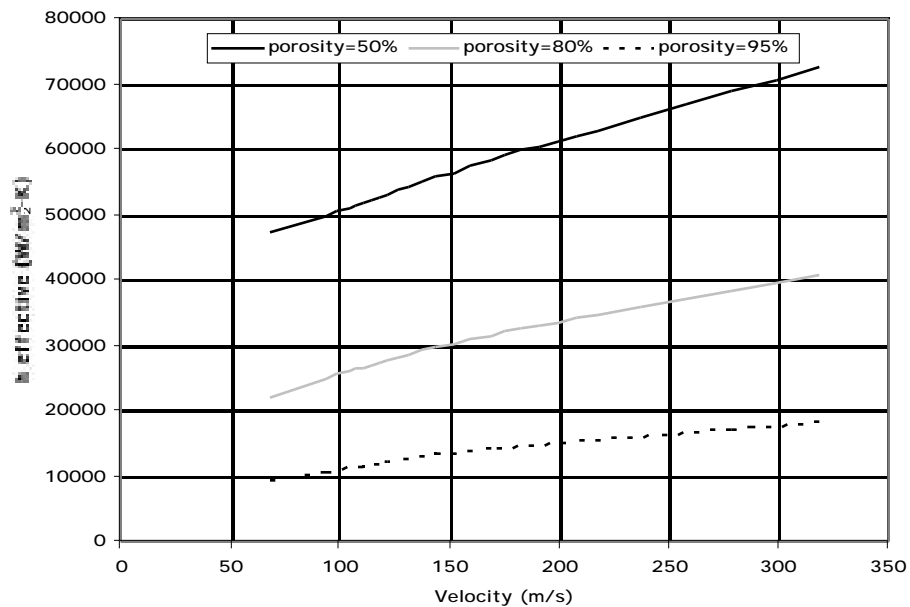


Figure 12 Effective heat transfer coefficient ($\text{W/m}^2\text{-K}$) at outlet as a function of velocity for different porosities ($q''=30 \text{ MW/m}^2$, $d_{\text{char}}=0.1 \text{ mm}$, $k_s=100 \text{ W/m-K}$, He $T_{\text{in}}=823\text{K}$).

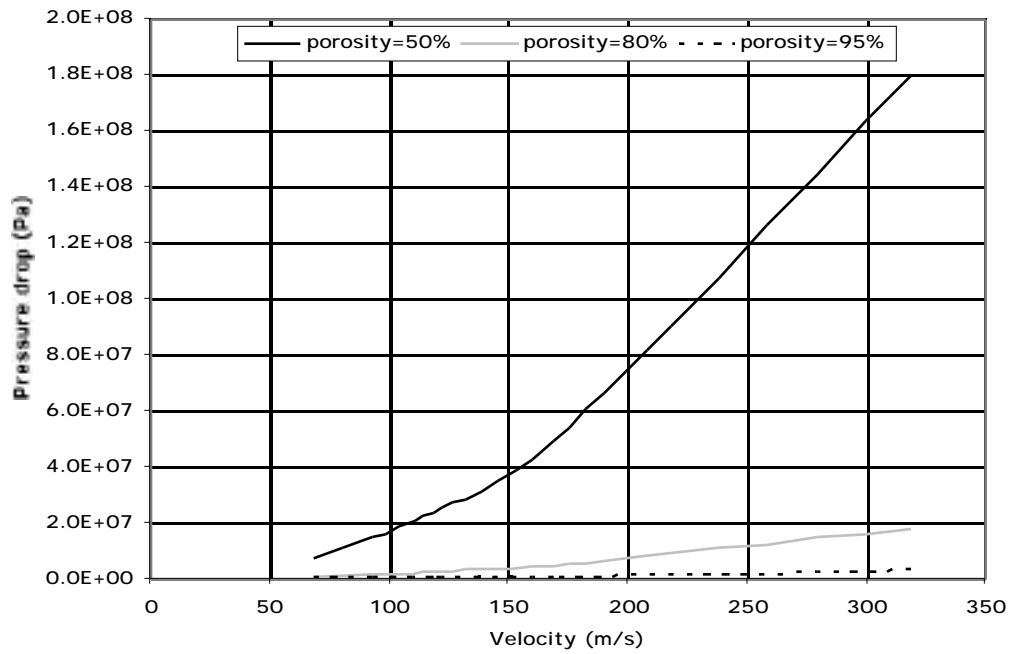


Figure 13 Pressure drop (Pa) as a function of velocity for different porosities ($q''=30$ MW/m², $d_{char}=0.1$ mm, He $T_{in}=823$ K).

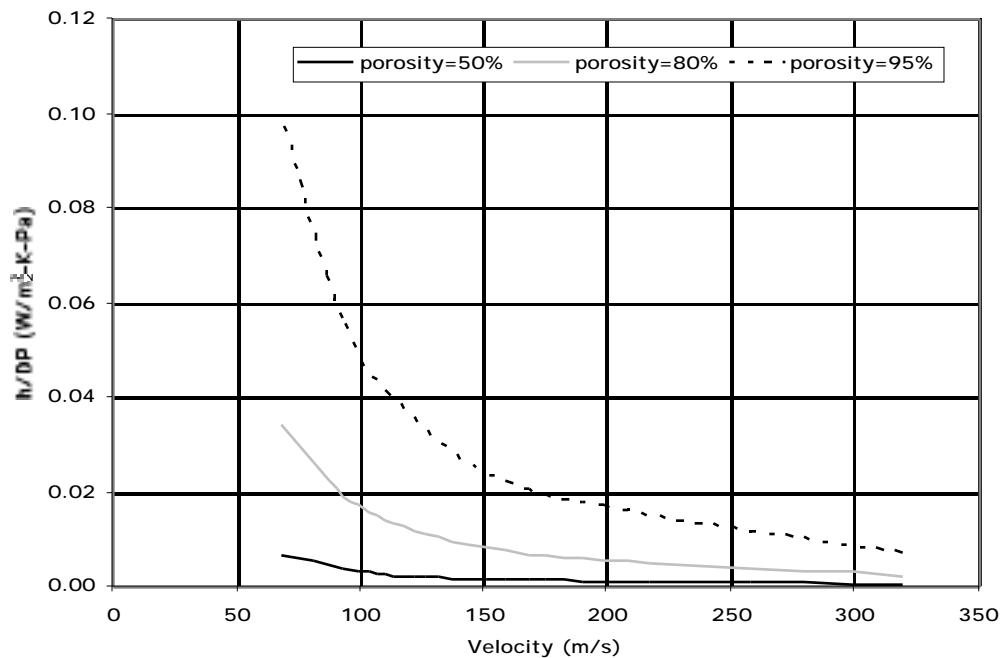


Figure 14 Ratio of effective heat transfer coefficient at outlet to pressure drop as a function of velocity for different porosities ($q''=30$ MW/m², $d_{char}=0.1$ mm, $k_s=100$ W/m-K, He $T_{in}=823$ K).

4.2.2 Porous Medium Characteristic Dimension and Channel Width

The porous medium characteristic dimension and channel width were then adjusted to understand their effect on the heat transfer performance and corresponding pressure drop. Figure 15 shows the variation of h_{eff} with the characteristic particle dimension for a heat flux of 5 MW/m^2 . The surface area to volume ratio decreases with increasing porous medium characteristic dimension, so the drop in the effective heat transfer coefficient for increasing porous medium characteristic dimension is expected. Decoupling the pebble bed relationship between surface area and characteristic particle dimension found in Equation (1) by tailoring the microstructure (as in a porous foam), should improve the heat transfer to pressure ratio considerably over that of conventional spherical particles. However, the exact geometry of such a microstructure has to be established through a combined fabrication feasibility and modeling analysis approach.

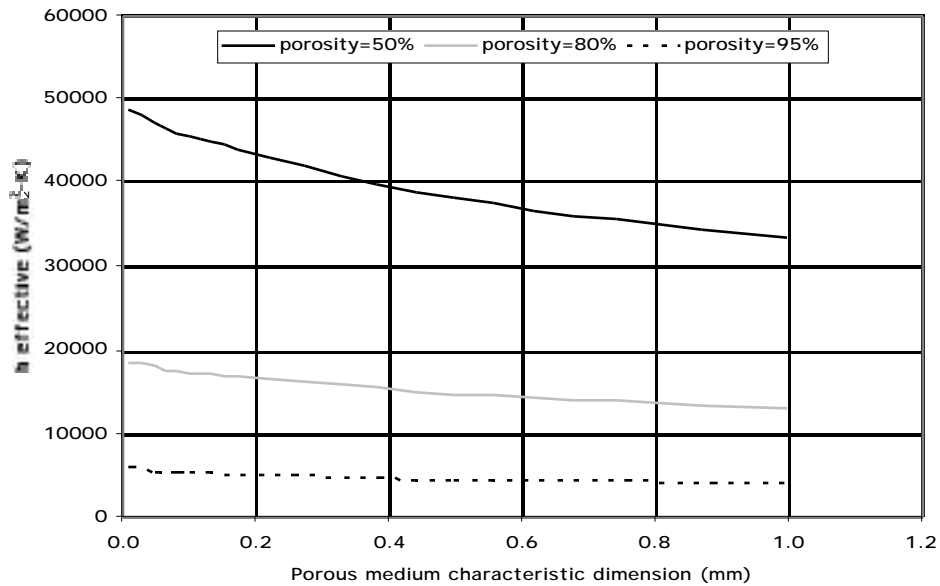


Figure 15 Effective heat transfer coefficient at outlet as a function of porous medium characteristic dimension for different porosities ($q''=5\text{MW/m}^2$, $k_s=100 \text{ W/m-K}$, He $T_{\text{in}}=823\text{K}$, He $T_{\text{out}}=1223\text{K}$).

Figure 16 shows that the pressure drop also decreases with increasing particle characteristic dimension. Figure 17 is a plot of h_{eff}/P as a function of particle dimension and shows that a larger characteristic dimension gives better results for the cases considered. This is probably more applicable to porous media approximating the shape of spherical particles or cylindrical fibers which better fit the model of permeability assumed for the analysis.

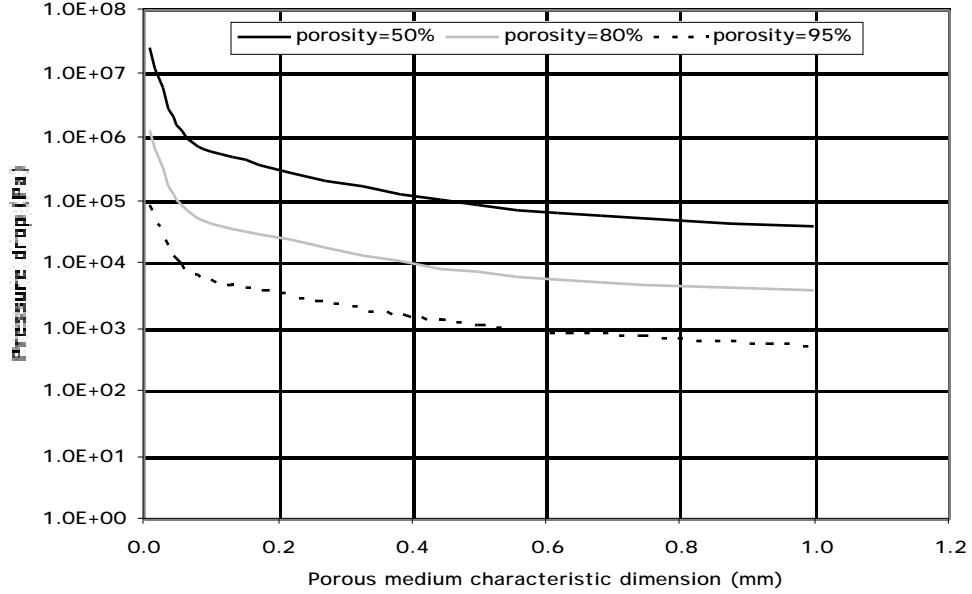


Figure 16 Pressure drop as a function of porous medium characteristic dimension for different porosities ($q''=5 \text{ MW/m}^2$, He $T_{in}=823\text{K}$, He $T_{out}=1223\text{K}$).

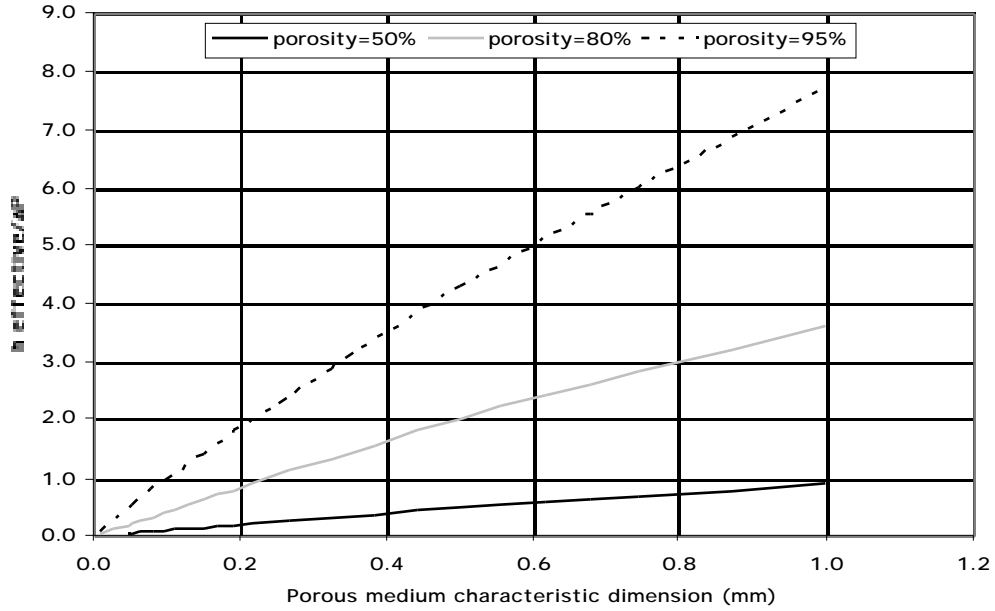


Figure 17 Ratio of effective heat transfer coefficient at outlet to pressure drop as a function of porous medium characteristic dimension ($q''=5 \text{ MW/m}^2$, $k_s=100 \text{ W/m-K}$, He $T_{in}=823\text{K}$, He $T_{out}=1223\text{K}$).

Finally, the effect on the heat transfer performance of changing the channel width while maintaining the same mass flow and pressure drop was investigated. In order to maintain the same mass flow for different sized channels, the velocity must be increased as the channel width is decreased. In order to maintain the same pressure drop for different channel widths, the porosity was adjusted (for a fixed porous medium characteristic dimension of 0.15 mm) to offset the increased pressure drop incurred from the increased velocity. Figure 18 illustrates the results. There is a definite advantage to a small channel dimension with a high porosity medium and high fluid velocity.

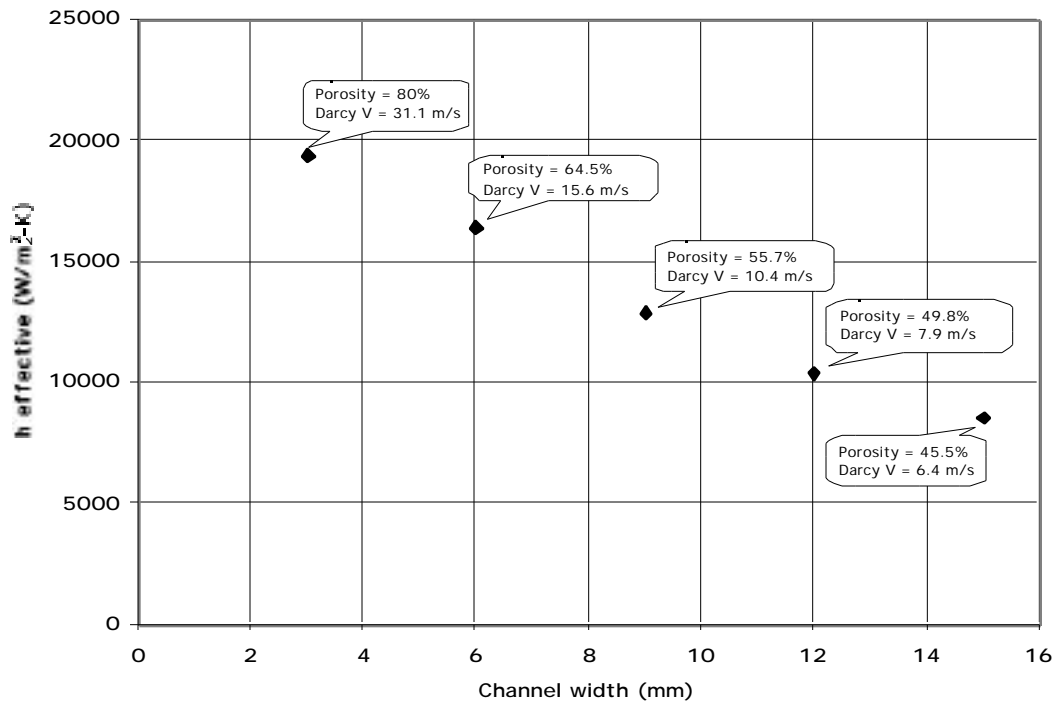


Figure 18 Effective heat transfer coefficient at outlet as a function of channel width for constant mass flow rate and pressure drop ($r_{out}=24\text{mm}$, $q''=5\text{ MW/m}^2$, $k_s=100\text{ W/m-K}$, He $T_{in}=823\text{K}$, He $T_{out}=1223\text{K}$).

4.2.3 Dispersion Effect and Solid/Fluid Heat Transfer Coefficient

The effect on the results of including dispersion was parametrically evaluated. Several cases were run with the dispersion model shown in Eq. (15) and the effect was found to be small in particular for higher porosity. For example, for the parameters listed in Table 1 with a He outlet temperature of 1223 K, a heat flux of 5 MW/m², solid thermal conductivity $k_s=100\text{ W/m-K}$, and a porosity of 0.8, the effective heat transfer coefficient is 17,190 W/m²-K without the effect of dispersion and 17,300 W/m²-K when including dispersion. For a lower porosity (0.5), the dispersion effect is somewhat more important with an effective heat transfer coefficient of 45,310 W/m²-K without the

effect of dispersion and $46,020 \text{ W/m}^2\text{-K}$ when including dispersion. Although the absolute h_{eff} value might be changed if the dispersion effect is included, the change would be small and the major findings from the above parametric studies would still apply. It would be interesting to try optimizing the porous microstructure characteristic to encourage dispersion and further help the heat transfer performance; however, this would have to be verified experimentally.

The effect on the results of varying the heat transfer coefficient between solid and flowing fluid, h_c , was also evaluated. For the same case as above, h_c from Eq. (13) is about $4,000 \text{ W/m}^2\text{-K}$. Cases were run with values higher by one order of magnitude ($40,000 \text{ W/m}^2\text{-K}$) and lower by one order of magnitude ($400 \text{ W/m}^2\text{-K}$). For the case with lower h_c , h_{eff} was calculated as $21,540 \text{ W/m}^2\text{-K}$ and $9,017 \text{ W/m}^2\text{-K}$ for porosities of 0.5 and 0.8, respectively. For the case with higher h_c , h_{eff} was calculated as $50,530 \text{ W/m}^2\text{-K}$ and $19,090 \text{ W/m}^2\text{-K}$ for porosities of 0.5 and 0.8, respectively. This suggests that h_c plays a larger role as the porosity increases. However, again, although the absolute h_{eff} values might change, the general observations from the parametric studies would still apply for different values of h_c .

4.3 Example Optimization for a Specific Divertor Case

An example application of the results from the above parametric studies is the determination of an attractive set of parameters for the ARIES-ST divertor case with an assumed tungsten armor thickness of 3-mm. The operating temperature range for tungsten is assumed to be from $\sim 973\text{-}1073\text{K}$ to 1673 K ($\sim 700\text{-}800^\circ\text{C}$ to $\sim 1400^\circ\text{C}$), which are consistent with the recommendations of Ref. [11], the lower limit being determined by irradiation embrittlement and the upper limit by loss of strength. For a design heat flux of 5 MW/m^2 and an assumed tungsten thermal conductivity of 100 W/m-K , the temperature drop through the W armor is about 150 K which when added to the maximum channel wall temperature would yield the maximum tungsten temperature. From the results shown in Fig. 9, the required velocities to maintain the maximum W temperature $< 1400^\circ\text{C}$ are about 11, 15 and 53 m/s for porosity values of 50%, 80% and 95%, respectively. From Fig. 11, the P 's corresponding to velocities of 11, 15 and 53 m/s and porosity values of 50%, 80% and 95% are 0.32, 0.07 and 0.07 MPa, respectively.

For the 30 MWm^2 case, the temperature drop for a 3-mm W wall is about 900 K leaving little room for a reasonable film drop to meet the requirement of a maximum W temperature of 1673 K . Thus, such a porous medium cannot satisfy the requirement unless very low porosity and very high pressure drop are allowed. However, if the W thickness is reduced to 1 mm , the maximum W

temperature can be maintained < 1673 K with velocities of about 60 m/s and 120 m/s for porosities of 50% and 80% respectively, as inferred from Fig. 12. From Fig. 13, the corresponding pressure drops are 7 MPa and 2 MPa, respectively.

Thus, a He-cooled W porous medium configuration seems to be a potentially attractive option for divertor application, being able to comfortably accommodate heat fluxes of ~ 5 MW/m² and possibly higher heat fluxes of up to 20-30 MW/m² but at the cost of higher pressure drops and higher system pressure, and/or of lower coolant inlet temperature and lower-quality heat extraction.

Conclusions

MERLOT, a comprehensive thermo-fluid model for flow through porous media has been developed. It is a versatile model enabling determination of effects of a number of different parameters, including: the porous medium characteristics, the fluid properties and design parameters, the solid conductivity, and the size of the channels. It has also the capability to account for local microstructure variation and to include potentially important processes such as the local heat transfer between solid and fluid and the effect of dispersion. Such a model provides an important tool to perform detailed assessment and optimization of porous media for high heat flux application, namely for a fusion divertor. It was used to perform detailed parametric studies to help in better assessing and optimizing porous media for high heat flux application. Specific and well characterized experimental results on such configurations are scarce and these parametric studies are very useful in determining key variables and in guiding future R&D.

The major observations from the results of the studies presented in this paper are summarized below:

- The local effective heat transfer coefficient (h_{eff}) is much higher at the entrance and decreases to a constant value as the flow becomes thermally developed. This indicates the attractiveness of designing for high heat flux accommodation close to the entrance region. However, when evaluating different configurations, the effective heat transfer coefficient at the coolant outlet should be chosen as a reasonable comparative measure of heat transfer performance.
- The solid thermal conductivity has an important effect on the effective heat transfer coefficient in particular at lower porosities. If allowed by the choice of solid material,

increasing the solid thermal conductivity is highly desirable since it does not adversely affect the pressure drop while increasing the effective heat transfer coefficient.

- An interesting performance to penalty measure is the ratio of effective heat transfer coefficient to pressure drop. This ratio is much higher at lower velocities and decreases rapidly with velocity, indicating the benefit of optimization at the lowest possible velocity for a given porosity. Interestingly, for a given velocity, it also indicates the benefit of optimization at the highest possible porosity as the ratio decreases sharply with decreasing porosity. The ratio of effective heat transfer coefficient to pressure drop also increases with increasing porous medium characteristic dimension. However, this is probably more applicable to porous media approximating the shape of spherical particles or cylindrical fibers which better fit the model of permeability assumed for the analysis.
- Decoupling the pebble bed relationship between surface area and characteristic particle dimension by tailoring the microstructure (as in a porous foam), would significantly improve the heat transfer to pressure ratio over that of a conventional particle bed. However, the exact geometry of such a microstructure has to be established through a combined fabrication feasibility and modeling analysis approach.
- Except in the case of change in solid thermal conductivity, the relative pressure drop penalty seems to be dominant over the corresponding enhancement in effective heat transfer coefficient when adjusting all other parameters considered, namely when increasing porosity, increasing velocity, and/or decreasing porous medium characteristic dimension. Therefore, a porous medium design will better optimize with parameters reducing the pressure drop indicating a strategy where the pressure drop should be minimized for a required heat transfer performance.
- Based on a strategy of fixing the pressure drop and adjusting the design parameters for maximum heat transfer performance, there seems to be a definite advantage to a small channel dimension with a high porosity medium and high fluid velocity. In simpler terms, it seems that a higher velocity is preferable to a lower porosity when maximizing the heat transfer performance for a given pressure drop.
- Isotropic porosity is not a requirement for metal foams or ordered fibers, but is a simplification that could later be lifted in order to experiment with deliberate porosity variation, or material tailoring.

- A He-cooled porous medium configuration seems to be an attractive divertor candidate concept, being able to comfortably accommodate heat fluxes of $\sim 5 \text{ MW/m}^2$ and possibly higher heat fluxes of up to $20\text{-}30 \text{ MW/m}^2$ but at the cost of higher pressure drops ($\sim 2 \text{ MPa}$ in the latter case) and higher system pressure, and/or of lower coolant inlet temperature and lower-quality heat extraction.
- The above observations are based on analysis results and would need to be confirmed experimentally. Dedicated experiments are required to better understand and characterize the key processes affecting the porous medium heat transfer performance. These experiments should cover a range of porosity, porous medium microstructure, velocity, channel dimension and flow path length to help determine the corresponding range of heat transfer performance and pressure drop, and to help in the optimization of the porous medium configuration best suited for divertor application. The experiments should be done in high heat flux facilities such as the electron gun at Sandia National Laboratory [3] over a range of heat fluxes ($\sim 5\text{-}30 \text{ MW/m}^2$) and with diagnostics enabling the measurement of the spatial temperature profile along the flow path in the porous media and in the channel wall as well as the characterization of all the key fluid parameters including the velocity profile (in particular for cases with spatial variation of porous medium microstructure). They also need to be done in parallel with porous medium material development for this application. In this regard, MERLOT is a very useful tool to help in specifying the attractive envelope of porous medium microstructure characteristics, and to help in planning the experiments, in interpreting the results and in applying them for divertor analysis.

Acknowledgement

This work was partially supported by grants from the University of California Energy Institute and from Plasma Processes Inc.

Nomenclature

A	shape factor
C	inertia coefficient
Cp_f	fluid heat capacity
Cp'_f	non-dimensional fluid heat capacity
$Cp_{f,ref}$	reference fluid heat capacity
d_{char}	porous medium characteristic dimension
d_p	particle diameter

Da	Darcy number
h_c	heat transfer coefficient for pebble bed
h_{eff}	effective heat transfer coefficient
h_p	particle-to-fluid heat transfer coefficient
h'_c	non-dimensional heat transfer coefficient
$k_{disp,r}$	enhancement of fluid thermal conductivity by dispersion, r-direction
$k_{disp,\theta}$	enhancement of fluid thermal conductivity by dispersion, θ -direction
k_f	fluid thermal conductivity
$k_{f,r}$	fluid thermal conductivity, r-direction
$k_{f,ref}$	reference fluid thermal conductivity
$k_{f,t,r}$	total effective fluid thermal conductivity, r-direction
$k_{f,t,\theta}$	total effective fluid thermal conductivity, θ -direction
k_p	porous medium thermal conductivity
k_s	solid thermal conductivity
$k_{s,r}$	solid thermal conductivity, r-direction
$k_{s,ref}$	reference solid thermal conductivity
$k_{s,\theta}$	solid thermal conductivity, θ -direction
k'_f	non-dimensional fluid thermal conductivity
k'_s	non-dimensional solid thermal conductivity
K	porous medium permeability
P	fluid pressure
P_{in}	fluid inlet pressure
P'	dimensionless pressure
P_0	reference pressure
Pr	Prandtl number
q'_f	non-dimensional fluid volumetric heat generation
q'_s	non-dimensional solid volumetric heat generation
q'_w	non-dimensional wall heat flux
q''_w	wall heat flux
$q''_{w,ref}$	reference wall heat flux
q'''_f	fluid volumetric heat generation
q'''_{ref}	reference volumetric heat generation
q'''_s	solid volumetric heat generation
r	coordinate
r_{in}	inner radius
r'	dimensionless radius
r_{out}	outer radius
R_o	porous medium-to-wall interface resistance
Re	Reynolds number of channel
Re_{dp}	Reynolds number w.r.t. particle dimension
S_{BET}	specific surface area
S_p	specific surface area
t	porous medium thickness
T_c	cold reference temperature
T_f	fluid temperature
T_h	hot reference temperature
T_{in}	Helium inlet temperature
T_{out}	Helium outlet temperature
T_s	solid temperature
T'_f	non-dimensional fluid temperature
T'_s	non-dimensional solid temperature
V_0	superficial velocity (1-D)

V_θ	superficial velocity in θ direction
V'_θ	dimensionless superficial velocity in theta direction
$V_{\theta,o}$	reference superficial velocity in theta direction
ε	average porosity
ε_i	local porosity
ε_{inf}	porosity at infinity (far from the wall)
P	fluid pressure drop
θ	coordinate
φ	particle shape factor
μ	fluid viscosity
ρ_f	fluid density
$\rho_{f,ref}$	reference fluid density
ρ'_f	non-dimensional fluid density
μ_{eff}	effective viscosity

References

1. J. H. Rosenfeld, Porous metal heat exchanger for cooling plasma-facing components, DoE SBIR Phase I Final Report, DE-FG05-92ER81645, June 1994.
2. J. H. Rosenfeld, J. E. Toth, and A. L. Phillips, Emerging applications for porous media heat exchangers, Proc. Int. Conf. on Porous Media and their Applications in Science, Kona, Hawaii, June 1996.
3. D. L. Youchison, M. G. Izenson, C. B. Baxi, J. H. Rosenfeld, High heat flux testing of helium-cooled heat exchangers for fusion applications”, Fusion Technology, Vol. **29** (no.4) July 1996, p.559-570.
4. M. S. Tillack, X. R. Wang, J. Pulsifer, S. Malang, D. K. Sze, M. Billone, I. Sviatoslavsky, and the ARIES Team, Fusion power core engineering for the ARIES-ST power plant, submitted for publication in Fusion Engineering and Design, 1999.
5. Andrew J. Sherman, Robert H. Tuffias, and Richard B. Kaplan, Refractory ceramic foams: A novel high temperature structure”, <http://www.ultramet.com/foamtech.htm>, 1999. See also A. J. Sherman, B. E. Williams, M. J. DelaRosa, and R. LaFerla, Characterization of porous cellular materials fabricated by CVD,” presented at the 1990 MRS Fall Meeting, Boston, MA, 26-30 November 1990.
6. D. A. Nield and A. Bejan, Convection in porous media, 2nd edition, Springer, New York, 1999.

7. D. A. Anderson, J. C. Tannehill and R. H. Pletcher, Computational fluid mechanics and heat transfer, Hemisphere Publishing Corporation, New York, 1984.
8. K. Kar and A. Dybbs, Internal heat transfer coefficients of porous media. Heat Transfer in Porous Media, Editors: J. V. Beck and L. S. Yao, HTD-22, ASME, 1982.
9. C. T. Hsu and P. Cheng, Thermal dispersion in porous medium,” Int. J. Heat Mass Transfer, Vol. 33, No. 8, pp1587-1597, 1990.
10. P. Cheng and C. T. Hsu, Fully-developed, forced convective flow through an annular packed-sphere bed with wall effects,” Int. J. Heat Mass Transfer, Vol. 29, No. 12, pp1843-1853, 1986.
11. S. Zinkle and L. Snead, “Materials Research and development for Fusion Energy Applications,” Oak Ridge National Laboratory, pre-print, private communication.